Electron beam treatment and hard anodic oxidation of AlSi7 alloys to improve the anodic oxide properties

Massimiliano Bestetti[1,2], Andrea Lucchini Huspek[1], Batuhan Akdogan[1], Yuriy H. Akhmadeev[3], Elizaveta A. Petrikova[3], Yuriy F. Ivanov[3], Pavel V. Moskvin[3], and Nikolay Koval[3]

[1]Politecnico di Milano, Dipartimento di Chimica, Materiali e Ingegneria "Giulio Natta"
20133, Piazza Leonardo da Vinci, 32, Italia
E-mail: *massimiliano.bestetti@polimi.it
[2]Tomsk Polytechnic University, The Weinberg Research Centre
634050, Tomsk, Lenin Ave., 2, bd. 4, Russia
[3]Institute of High Current Electronics, Siberian Branch of Russian Academy of Science (IHCE SB RAS)
634055, Tomsk, Akademichesky Ave., 2/3, Russia
DOI: 10.31554/978-5-7925-0655-8-2023-175-182

Al-Si alloys are among the most common aluminium-based cast products due to their high strength-to-weight ratio, excellent processability and relatively low cost. Their surface mechanical properties and corrosion resistance are usually enhanced by forming a protective anodic oxide coating by means of hard anodic oxidation. However, the presence of silicon particles within the aluminium matrix decreases the quality and integrity of the anodic oxide. In the present work, RITM-SP and SOLO electron beam facilities are used to modify the distribution of silicon in the surface region of the alloy. The hard anodic oxides produced after electron beam pre-treatment were characterized by SEM-EDS and in term of corrosion resistance properties.

Introduction

Aluminium alloys are widely used in several industrial fields due to their high strength-to-weight ratio, good thermal and electrical conductivity and excellent processability. The addition of Si to the melt improves the castability of the molten alloy and reduces the solidification shrinkage, improves the corrosion and wear resistance of Al-Si alloys, making the Si one of the most commonly employed elements in combination with Al [1]. Al-Si alloys typically contain from 3 to 20 wt.% of silicon, being divided in hypoeutectic, eutectic (12,6%) and hypereutectic.

Even though Al tends to form spontaneously a native thin oxide which passivates the surface, anodic oxidation is frequently employed to form a thick coating which improves surface mechanical properties and corrosion resistance. Among the different Al-Si foundry alloys, the response of hypoeutectic Al-Si with respect to anodization is widely studied [2]. The growth of the oxide layer, as well as its final characteristics, are strongly affected by the microstructure of the alloy: the presence of Si particles in the α-Al matrix drastically impairs the homogeneity and the integrity of the anodic oxide coating. In fact, Si particles have a slower oxidation rate with respect to Al matrix, making more favourable the formation of Al_2O_3 with respect to SiO_2. Silicon particles with diameter smaller than few μm are not considered as deleterious for the continuity of oxide layer. Instead, larger particles cause different flaws such as porosities, unoxidized areas and cracks [2].

In the present work, two different low energy high current electron beam facilities (LEHCEB), namely RITM-SP and SOLO, were used to modify the surface distribution of Si in the alloy. The aim is to refine and distribute Si particle in Al matrix and, as a consequence, to get beneficial effects on the growth of a hard anodic oxide layer, obtaining a more homogenous coating with less defects.

Materials and Methods

Samples (20×20 mm) were cut from gravity casted ingots, nominally of AlSi7 (EN-AC-42200) alloys. They were mechanically polished (100, 320 and 600 grit), ultrasonically washed in 50 vol% acetone and 50 vol% ethanol for 15 minutes, rinsed in deionized water and dried with nitrogen.

A first set of samples was electron beam treated in a RITM-SP facility [3, 4]. Base pressure reached $2.0 \cdot 10^{-5}$ torr and argon working pressure was set at $2.0 \cdot 10^{-4}$ torr. Electron accelerating voltages were set at 20 and 25 kV, corresponding to the energy densities of 2.5

and 3.3 J/cm^2, respectively. The number of pulses were 2, 4, 8, 16 and 32, with pulse average duration of 2.5 µs at 0.2 Hz of repetition frequency. The second set of samples was electron beam treated with SOLO equipment [5, 6] and the energy densities used were 10, 15, 20, 25 and 30 J/cm^2 and the number of pulses was set to 3 at repetition frequency of 0.3 Hz with the average pulse duration of 200 µs.

Hard anodic oxidation was carried out in a jacketed glass reactor by using a 17.5% v/v H_2SO_4 aqueous solution. Temperature was kept a 0 °C (±1 °C) using a Julabo FP50 cryostat. A titanium mesh was employed as a cathode, being the ratio between cathode and anode areas equal to 3:1. The distance between cathode and anode was 30 mm and the applied current density was 2 A/dm^2.

The morphology was investigated using a Zeiss EVO 50VP SEM equipped with a Bruker X-ray spectrometer for chemical microanalysis (EDS). The crystalline structure was characterized by X-ray diffraction in grazing angle configuration (GI-XRD) using a PANalytical EMPYREAN PW1830 diffractometer. Surface hardness was measured using a Shimadzu HMV-2000 Vickers microindenter by applying a 10 g load. Corrosion potential and corrosion current density were measured using AMEL 2049 potentiostat in 3.5% NaCl solution at room temperature. A three-electrode cell was employed with Al-Si sample as WE, a platinum mesh as CE and a saturated calomel electrode (AMEL) as REF. At first, open circuit potential was measured for 30 minutes with acquisition rate of 1 Hz. Then, a potentiodynamic test was performed from -250 mV to +250 mV with respect to OCP at a scan rate of 10 mV/min.

Results and discussion

RITM-SP facility

At first, samples were characterized by means of SEM and elemental distribution was assessed by EDS. Figure 1 shows the surface morphology of the as-polished sample and that of samples treated at 20 kV with 8, 16 and 32 pulses. After RITM-SP treatment, the surface appears smoother and more homogeneous. This effect is more pronounced as the number of pulses increases. During the electron beam irradiation with RITM-SP facility, a surface layer of few µm is molten and then rapidly solidified, causing a change of the microstructure. In figure 1, spherical features are visible, especially in samples with a low number of pulses, in correspondence of which a higher EDS signal of oxygen was detected. The number of such spherical particles and their size decreases at 16 and, especially, 32 pulses, as shown in figures 1c and 1d. In EDS maps, displayed in figure 2, the shape and size silicon segregations in the matrix agree with typical metallographic images of hypoeutectic Al-Si alloys [7].

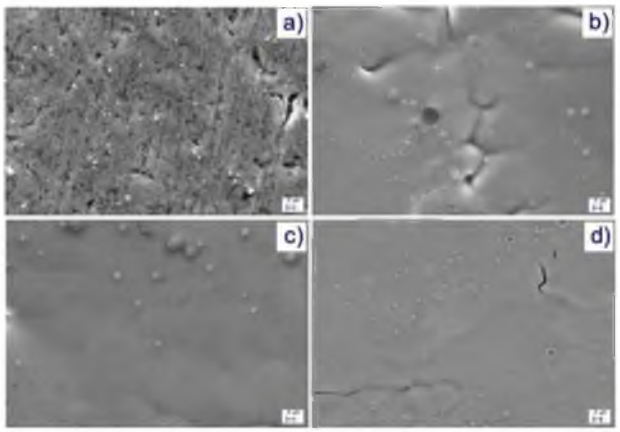

Fig.1. SEM surface morphology of: a) pristine and b) c), d) 20 kV samples at 8, 16 and 32 pulses, respectively.

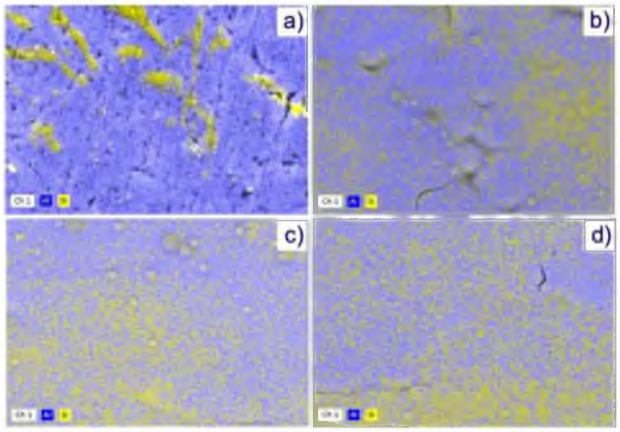

Fig.2. Surface Al (blue) and Si (yellow) EDS maps of: a) pristine and b) c), d) 20 kV samples at 8, 16 and 32 pulses, respectively.

Figures 2b, 2c and 2d show the change in the silicon distribution induced by RITM-SP treatment: instead of localized silicon segregations, a more homogeneous and uniform dispersion is obtained. This modification is induced by a rapid melting and solidification of the alloy surface during electron beam irradiation. Moreover, according to Si wt.% EDS

measurements, some of the silicon is evaporated from the surface leading to final measured values of 8.32% (16 pulses) and 7.62% (32 pulses), with respect to the pristine sample at 10.2%.

Computational modelling, not reported here, confirmed this finding which is mainly related to the difference in the thermal properties between aluminium and silicon. Figures 3 and 4 display the morphology and the EDS maps of samples treated at 25 kV with 8, 16 and 32 pulses. Surface appears smoother and more homogenous with respect to the treatment at 20 kV. EDS maps confirmed the dispersion of silicon aggregates: the treatment at 25 kV, especially at 16 and 32 pulses, led to an even higher diffusion of Si into Al matrix. Moreover, the content of Si decreased furthermore (4.36% after 32 pulses) with respect to 20 kV samples, indicating a more pronounced loss of silicon.

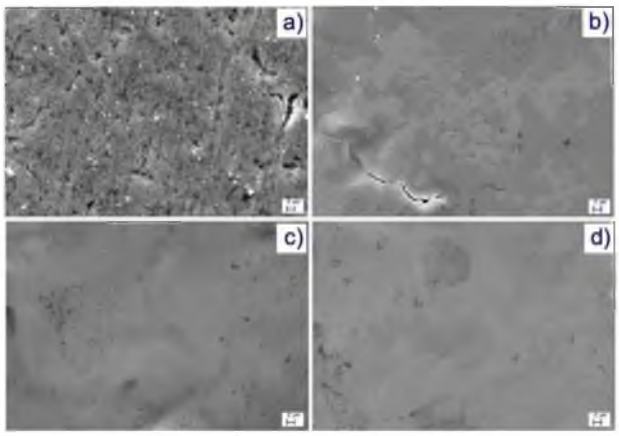

Fig.3. SEM surface morphology of: a) pristine and b) c), d) 25 kV samples, respectively at 8, 16 and 32 pulses.

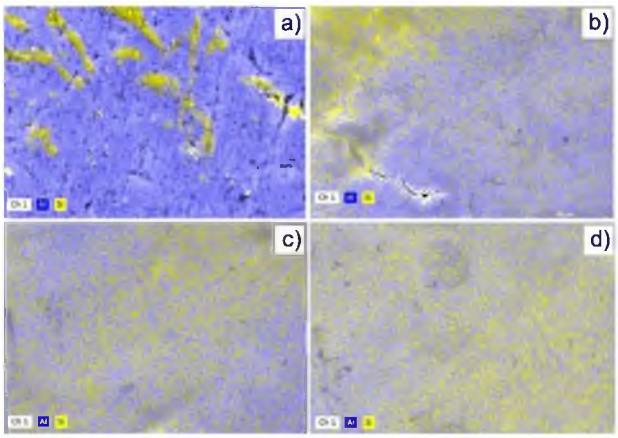

Fig.4. Surface Al (blue) and Si (yellow) EDS maps of: a) pristine and b) c), d) 25 kV samples at 8, 16 and 32 pulses, respectively.

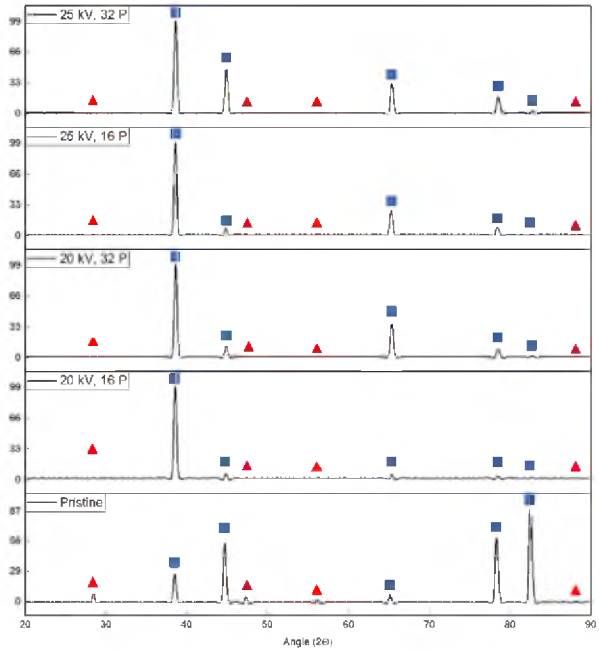

Fig.5. XRD spectra of RITM-SP samples: Al matrix peaks with blue squares, Si peaks with red triangles.

Samples were characterized by XRD in grazing angle configuration. Figure 5 shows the XRD spectra of samples treated with RITM-SP with different operating parameters. Peaks belonging to the structure of Si and those belonging to the Al matrix are highlighted. The intensity of the silicon peaks is close to zero as the energy density and the number of pulses increases, confirming the loss of Si particles and their partial dispersion in the Al matrix. On the other hand, a change in relative intensity of peaks of Al matrix is due to a change of crystallographic orientation of the sample. Peak fitting was then employed to calculate lattice parameters. The change of the lattice parameter of Al phase was linked to the amount of dissolved Si in the solid solution, according to [8]:

$$a(nm) = 0.40491 - 0.0174 x_{Si} - 0.0144 x_{Si}^2$$

where a is the lattice parameter of Al phase and x_{Si} is the wt.% of silicon in the solid solution. The fast quenching from the liquid state of Al-Si alloy led to the formation of a supersaturated solid solution. The maximum equilibrium solubility is 1.65% of Si at the eutectic temperature (577°C) [9]. Obtained values for 20 and 25 kV samples, and trendline with respect to number of pulses are reported in figure 6. The contribution of grain refinement, residual stresses and other alloying elements were not

considered. In conclusion, part of the initial Si in the as-casted alloy was evaporated from the surface layer, some of it was finely dispersed inside Al matrix and some was effectively brought in solid solution with Al.

Finally, before the anodic oxidation, the microhardness of samples was measured and results are displayed in figure 7. Depending on the sample, the penetration of the indenter was kept in the range of few micrometres in order to appreciate the thin surface layer modified by RITM-SP.

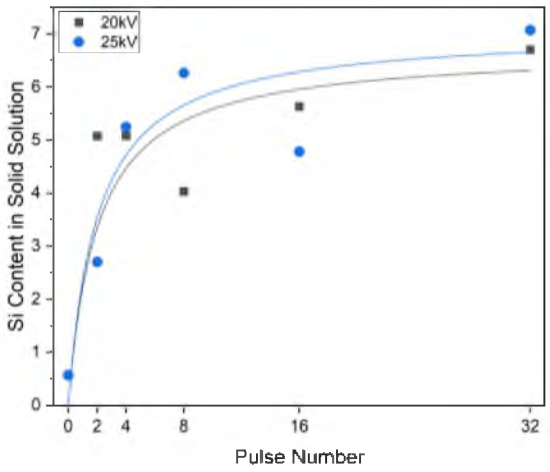

Fig.6. Silicon content in the aluminium solid solution as a function of number of pulses for two accelerating voltages.

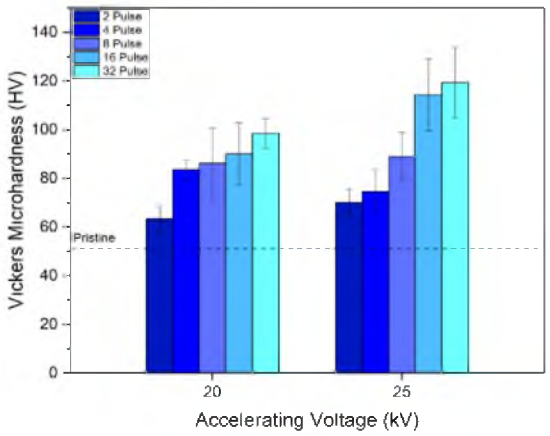

Fig.7. Vickers microhardness of RITM-SP samples in comparison with the pristine AlSi7 alloy (dashed line).

The pristine AlSi7 alloy gave a microhardness value of 51.5 ± 2.7 HV, in agreement with literature values [10]. The increase in surface hardness can be ascribed both to grain size refinement, calculated with Sherrer formula, and to the formation of supersaturated solid solution during the fast quenching of the material from the liquid state. A higher number of pulses is capable of inducing a stronger increase in surface microhardness, due to a better homogenization of the modified layer and, at the same time, a higher thickness of the modified layer. The difference in microhardness at low number of pulses, 4 and 8, is not remarkable when comparing the samples at 20 and 25 kV. In conclusion, RITM-SP treatment allowed to increase surface microhardness by a factor of more than two.

Three selected samples were subjected to anodic oxidation: the aim was to compare the effect of different operating parameters on the anodic oxide properties: 25 kV/16 P, 25 kV/32 P and 20 kV/32 P. Figure 8 displays the cell voltage as a function of time: within the first 30 seconds the voltage increases remarkably before reaching steady state value, followed by a slight increase in the last minutes. The steady state cell voltage is slightly different for each of the treated samples even though the applied current density is the same. This behaviour is ascribed to a different composition and microstructure of the Al-Si alloys from which the anodic oxide is grown.

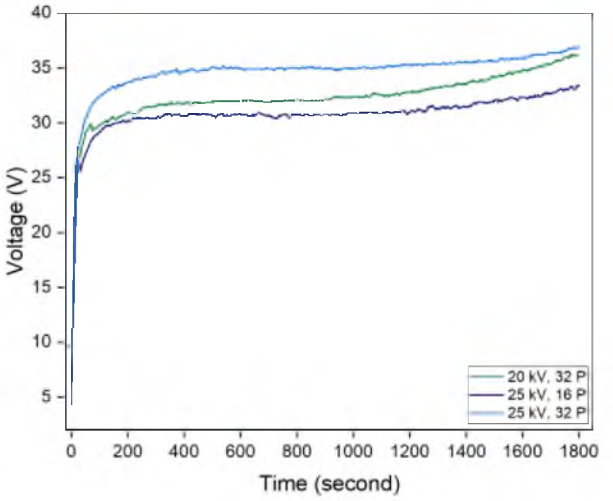

Fig.8. Cell voltage-time curves during hard anodic oxidation of RITM-SP treated AlSi7 samples.

Then, electrochemical measurements were employed to assess the behaviour of oxides in a standard aggressive solution. Table 1 reports the mean values of open circuit potential, corrosion current and corrosion potential obtained using the Tafel extrapolation from potentiodynamic test data.

Tab.1. Comparison between average open circuit potential, corrosion potential and corrosion current density of oxidized samples.

Sample	OCP (V *vs* SCE)	E_{corr} (V *vs* SCE)	i_{corr} ($\mu A/cm^2$)
Pristine	-0.72	-0.67	0.65
25 kV 16 P	-0.78	-0.77	0.34
20 kV 32 P	-0.78	-0.75	0.80
25 kV 32 P	-0.77	-0.74	0.89

Beneficial effects were found in the 25 kV/16 P sample, with a decrease in corrosion current density of 0.31 $\mu A/cm^2$ with respect to pristine Al-Si oxide. In the other cases, the corrosion current density was slightly higher, implying that the anodic oxide layer is not much more protective with respect to the pristine Al-Si oxide. The cross-section comparison between the oxides grown on the pristine Al-Si alloy and the sample at 25 kV/16P is reported in figure 9. The electron beam irradiation slightly decreased the growth of the oxide, which has a lower thickness with respect to the one of pristine Al-Si. However, the coating produced from RITM-SP sample is more homogeneous, compact and with less defects caused by the presence of Si particles. EDS microanalysis confirmed the effectiveness of the dispersion of silicon phase due to RITM-SP treatment.

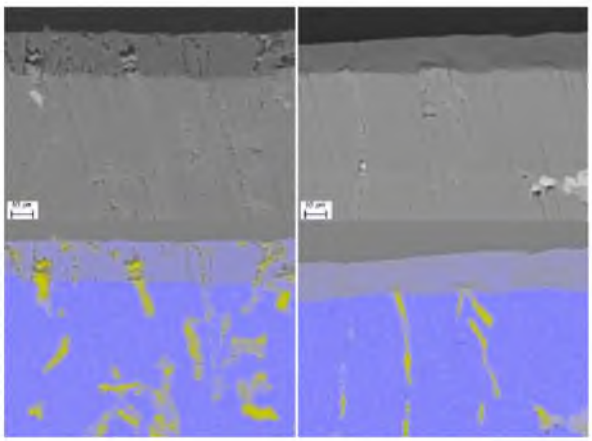

Fig.9. SEM cross-section and EDS maps (Al blue, Si yellow) of oxidized Al-Si alloys: untreated (left) and 25 kV/16P (right).

SOLO facility

Figure 10 shows the surface morphology of as-polished alloy and that of samples treated with 20, 25 and 30 J/cm^2. The modification induced at lower energy densities (10, 15 and 20 J/cm^2) interested almost only the aluminium matrix, bringing at the surface silicon segregations and making them more pronounced. The large difference between the melting temperatures and the thermal conductivities of Al and Si suggests that at low energy densities the electron beam treatment bring to the molten state only the aluminium matrix, leaving the silicon and other inclusions unmodified. However, by increasing the energy density up to 25 and 30 J/cm^2, similar results with respect to RITM-SP samples are found. In fact, the surface is smoothened and clearly reached a higher homogeneity. The absence of microcracks and porosities confirmed the excellence of the treatment. Moreover, any morphological features related to Si particles cannot be found anymore. EDS maps in figure 11 show that at 20 J/cm^2 a sharp distinction between Al matrix and Si particles is found. Instead, a finer and more homogeneous distribution of silicon is found in the samples irradiated with higher energies, as for the RITM-SP equipment. Then, according to the EDS analysis, a high amount of silicon was evaporated from the surface leading to a measured value of 5.15% (25 J/cm^2) and 5.55% (30 J/cm^2), with respect to 9.57% of pristine Al-Si. Figure 12 displays the cross-section morphologies and elemental maps of samples treated with 25 and 30 J/cm^2: a remarkably thick layer (15 and 35 µm, respectively) was found to be drastically modified by the SOLO electron beam irradiation. The material is smoothened and homogenized from a morphological point of view, and at the same time silicon EDS signal is almost vanished. The SOLO treatment proved to be, as a consequence, effective in dispersing and homogenizing Si particles in Al matrix, up to a thickness unattainable with RITM-SP facility.

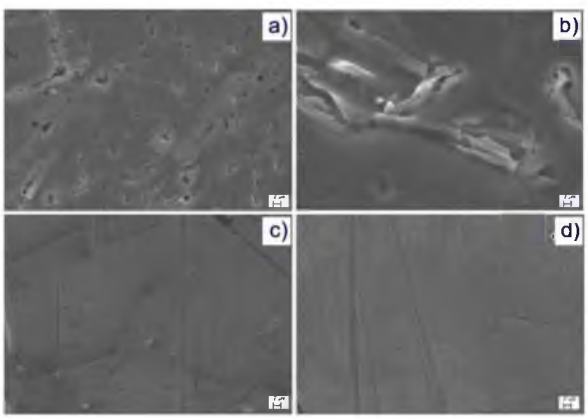

Fig.10. SEM surface morphology of: a) pristine and b) c), d) 20, 25 and 30 J/cm^2 treated with SOLO.

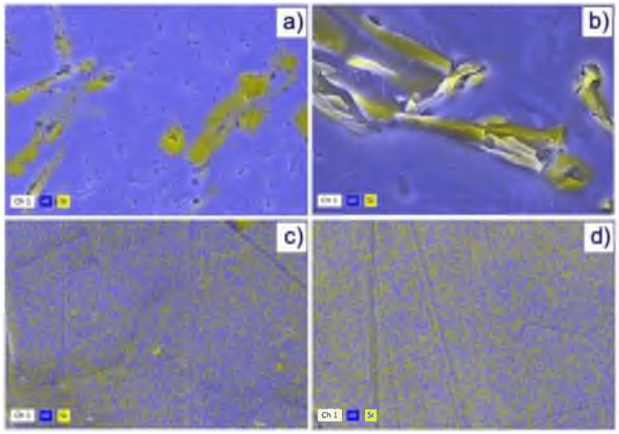

Fig.11. Surface Si and Al EDS maps of: a) pristine and b) c), d) 20, 25 and 30 J/cm^2 treated with SOLO.

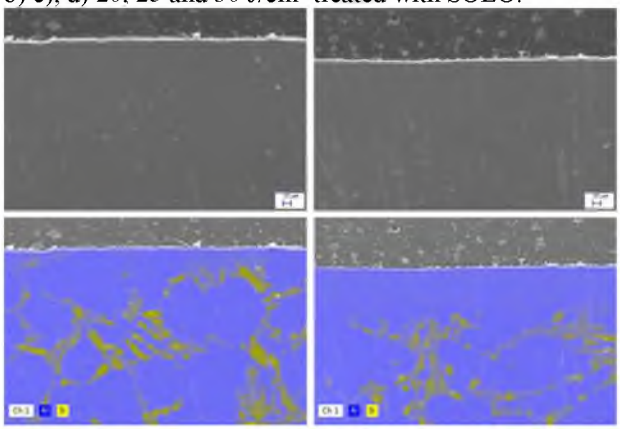
Fig.12. SEM cross-section morphology and EDS maps of SOLO Al-Si samples treated with 25 (left) and 30 J/cm^2 (right).

X-ray diffraction was employed to characterize the crystalline structure of samples: blue peaks are referred to the aluminium phase, while red ones to the silicon. Results displayed in figure 13 are quite similar to the spectra in figure 5. In fact, increasing the energy density, a change in crystallographic orientation of the Al grains is found and a sharp decrease of intensity of peaks associated to Si is observed. The preferential orientation of aluminium is along (111) ($2\theta = 38.6°$) direction as for RITM-SP samples. Moreover, the only remaining Si peak is associated to (111) direction as well ($2\theta = 28.3°$). Calculation of the lattice constants, which is not reported here, allowed to conclude that especially for high energy densities (25 and 30 J/cm^2) the lattice parameter of Al solid solution is lowered. As a consequence, by increasing the energy density above 20 J/cm^2 a higher amount of silicon is brought into the solid solution.

Microindentation was then used to assess the surface hardness and figure 14 displays the results. Energy densities per pulse from 10 to 20 J/cm^2 did not induce any remarkable changes in surface mechanical properties of AlSi7 alloy. Even though the energy density is much higher than RITM-SP, the longer pulse duration probably led to less pronounced thermal gradients, both in the heating and cooling phase, thus not modifying surface hardness. Instead, at 25 and especially 30 J/cm^2, a sharp increase of microhardness is observed. The maximum obtained value was 105.9 ± 11.5 HV, which is close to that obtained with RITM-SP treatment at 25 kV and 16 pulses. This means that a Vickers microhardness increase of more than two times was obtained with SOLO facility.

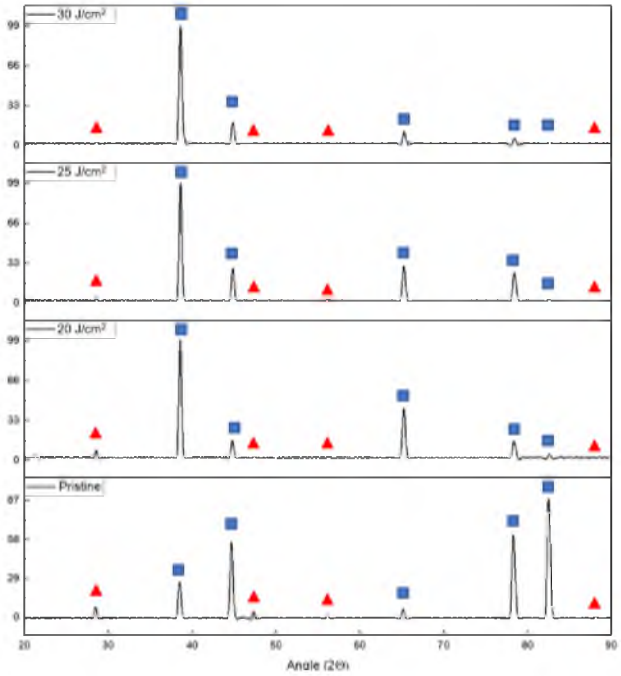

Fig.13. XRD spectra of pristine AlSi7, and of samples electron beam irradiated with SOLO at 20, 25 and 30 J/cm^2.

The anodic oxidation of samples treated with SOLO followed the same procedure used in the case of RITM-SP samples. Cell voltage *vs* time plots for 20, 25 and 30 J/cm^2 are reported in figure 15. Voltage is quickly raised up in the first few seconds of the oxidation and then constantly increases up to the end of the experiment: with respect to the previous set of samples, are slightly higher with respect to the ones obtained during the anodic oxidation of RITM-SP samples.

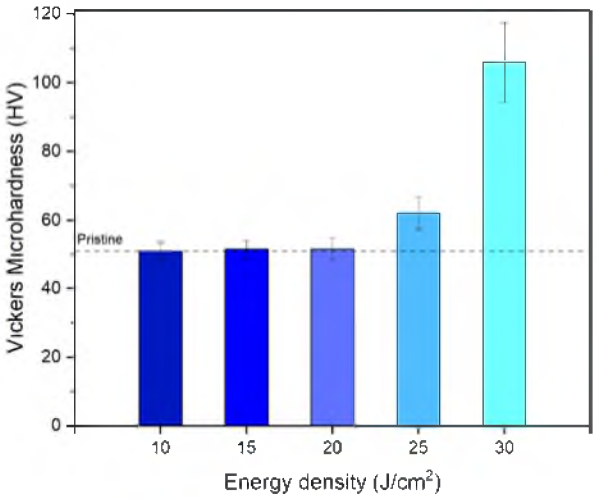

Fig. 14. Vickers microhardness of SOLO samples in comparison with the pristine AlSi7 alloy (dashed line).

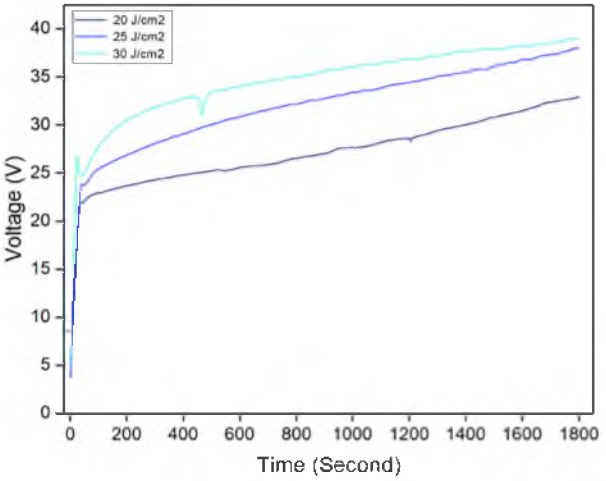

Fig.15. Cell voltage-time curves during hard anodic oxidation of SOLO treated AlSi7 samples.

The oxidized samples were tested in a standard three-electrode setup cell as previously described. Table 2 displays a comparison between the mean value of open circuit potential, corrosion current and corrosion potential obtained using the Tafel extrapolation.

Tab.2. Comparison between average open circuit potential, corrosion potential and current for SOLO samples.

Sample	OCP (V *vs* SCE)	E_{corr} (V *vs* SCE)	i_{corr} (μA/cm^2)
Pristine	-0.72	-0.67	0.65
20 J/cm^2	-0.76	-0.71	0.24
25 J/cm^2	-0.75	-0.76	0.17
30 J/cm^2	-0.73	-0.82	0.10

A decrease of corrosion current density was observed with respect to the untreated Al-Si anodized sample: the lowest values found was 0.1 μA/cm^2 for an applied energy density of 30 J/cm^2, which is six times lower in comparison with pristine Al-Si oxide (0.65 μA/cm^2). Figure 16 shows the cross-sections of oxides grown on as-produced Al-Si alloy and after SOLO treatment at 30 J/cm^2. As for RITM-SP treated samples, the coating is slightly thinner than pristine AlSi7. Moreover, the oxide coating is more homogeneous and compact compared to the reference one. In the case of SOLO samples, the oxidized thickness was thinner with respect to the electron beam modified layer, suggesting the possibility to grow even thicker but still homogeneous oxides.

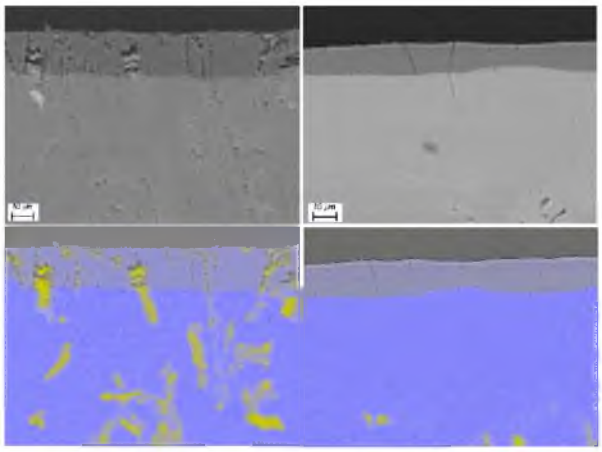

Fig.16. SEM cross-section and EDS maps (Al blue, Si yellow) of oxidized Al-Si alloys: untreated (left) and 30 J/cm^2 (right).

Conclusions

In the present work, two electron beam facilities, namely RITM-SP and SOLO, were employed for the modification of the surface of AlSi7 alloy samples. Surface morphology investigations revealed that both electron sources are able to induce an effective dispersion of silicon in the alloy, up to 35 μm in depth for the SOLO equipment. Silicon surface evaporation was confirmed by means of EDS analysis. XRD was employed to characterize the crystalline structure of samples: a sharp decrease in intensity of Si peaks was found, as well as a grain reorientation of the Al as a consequence of fast melting and solidification. Moreover, Si was effectively brought inside a supersaturated solid solution with Al. Surface microhardness was then measured: RITM-SP was able to induce the more pronounced increase in surface mechanical properties with different combinations of pulse numbers and accelerating voltages, SOLO techniques proved to be likewise val-

id allowing for two times increase of Vickers microhardness at 30 J/cm^2.

After electron beam irradiation, samples were subjected to hard anodic oxidation and their corrosion behaviour was assessed. Oxides grown onto RITM-SP treated samples showed a decrease of the corrosion current for intermediate number of pulses. On the other hand, a clearer trend was observed with SOLO samples: in this case corrosion current was decreased to the 15% of the original value.

Cross sections of the oxides were done to investigate the morphology of the coatings. Electron beam treatments, both RITM-SP and SOLO, allowed the growth of oxides more homogenous, compact and free of Si segregation, with respect to the as-cast AlSi7 alloy. In conclusion, the present work confirmed that a remarkable improvement of the quality of anodic oxide can be obtained by pre-treating AlSi7 alloys with RITM-SP and SOLO electron beams.

References

[1] Runge, J. M. The metallurgy of anodizing aluminium // *Cham: Springer International Publishing*, 2018.

[2] Scampone, G., & Timelli, G. Anodizing Al–Si foundry alloys: a critical review // *Advanced Engineering Materials*, *24*, 2101480, 2022.

[3] Proskurovsky, D. I., Rotshtein, V. P., Ozur, G. E., Ivanov, Y. F., & Markov, A. B. Physical foundations for surface treatment of materials with low energy, high current electron beams // *Surface and Coatings Technology*, *125*(1-3), 49-56, 2000.

[4] Rotshtein, V., Ivanov, Y., & Markov, A. Surface treatment of materials with low-energy, high-current electron beams // *Materials surface processing by directed energy techniques*, 205, 2006.

[5] Ashurova, K. T., Vorobyov, M. S., Petrikova, E. A., Ivanov, Y. F., Moskvin, P. V., & Rygina, M. E. Surface modification of hypereutectic silumin subjected to a millisecond modulated electron beam treatment // *Journal of Physics:* Vol. 2064, No. 1, p. 012045, IOP Publishing, 2021.

[6] Ustinov, A., Klopotov, A., Ivanov, Y., Zagulyaev, D., Teresov, A., Petrikova, E., Chumaevskii, A. Deformation Inhomogeneities of a Hypoeutectic Aluminium-Silicon Alloy Modified by Electron Beam Treatment // *Materials*, *16*(6), 2329, 2023.

[7] Saini, N., Dwivedi, D. K., Jain, P. K., & Singh, H. Surface modification of cast Al-17% Si alloys using friction stir processing // *Procedia Engineering*, *100*, 1522-1531, 2015.

[8] Bendijk, A., Delhez, R., Katgerman, L., De Keijser, T. H., Mittemeijer, E. J., & Van Der Pers, N. M. Characterization of Al-Si-alloys rapidly quenched from the melt // *Journal of Materials Science*, *15*, 2803-2810, 1980.

[9] Asensio-Lozano, J., & Vander Voort, G. The Al-Si Phase Diagram // *Tech notes*, *5*, 5, 2009.

[10] Lattanzi, L., Di Giovanni, M. T., Giovagnoli, M., Fortini, A., Merlin, M., Casari, D., & Garagnani, G. L. Room temperature mechanical properties of A356 alloy with Ni additions from 0.5 wt to 2 wt% // *Metals*, *8*(4), 224, 2018.